Article

Direct experimental constraints on the spatial extent of a neutrino wavepacket

https://doi.org/10.1038/s41586-024-08479-6

Received: 5 April 2024

Accepted: 3 December 2024

Published online: 12 February 2025

Open access

Check for updates

Joseph Smolsky[1]✉, Kyle G. Leach[1,2]✉, Ryan Abells[3], Pedro Amaro[4], Adrien Andoche[5], Keith Borbridge[1], Connor Bray[1,6], Robin Cantor[7], David Diercks[8], Spencer Fretwell[1], Stephan Friedrich[6], Abigail Gillespie[1], Mauro Guerra[4], Ad Hall[7], Cameron N. Harris[1], Jackson T. Harris[9], Leendert M. Hayen[10], Paul-Antoine Hervieux[5], Calvin Hinkle[1], Geon-Bo Kim[6], Inwook Kim[6], Amii Lamm[1], Annika Lennarz[3,11], Vincenzo Lordi[6], Jorge Machado[4], Andrew Marino[1], David McKeen[3], Xavier Mougeot[12], Francisco Ponce[13], Chris Ruiz[3], Amit Samanta[6], José Paulo Santos[4], Caitlyn Stone-Whitehead[1], John Taylor[1], Joseph Templet[1], Sriteja Upadhyayula[3], Louis Wagner[2,3] & William K. Warburton[9]

Despite their high relative abundance in our Universe, neutrinos are the least understood fundamental particles of nature. In fact, the quantum properties of neutrinos emitted in experimentally relevant sources are theoretically contested[1–4] and the spatial extent of the neutrino wavepacket is only loosely constrained by reactor neutrino oscillation data with a spread of 13 orders of magnitude[5,6]. Here we present a method to directly access this quantity by precisely measuring the energy width of the recoil daughter nucleus emitted in the radioactive decay of beryllium-7. The final state in the decay process contains a recoiling lithium-7 nucleus, which is entangled with an electron neutrino at creation. The lithium-7 energy spectrum is measured to high precision by directly embedding beryllium-7 radioisotopes into a high-resolution superconducting tunnel junction that is operated as a cryogenic sensor. Under this approach, we set a lower limit on the Heisenberg spatial uncertainty of the recoil daughter of 6.2 pm, which implies that the final-state system is localized at a scale more than a thousand times larger than the nucleus itself. From this measurement, the first, to our knowledge, direct lower limit on the spatial extent of a neutrino wavepacket is extracted. These results may have implications in several areas including the theoretical understanding of neutrino properties, the nature of localization in weak nuclear decays and the interpretation of neutrino physics data.

Quantum mechanics is based on the concept that the microscopic scale of our Universe contains inherent uncertainties in position and momentum that are fundamentally connected as $\sigma_x\sigma_p \geq \hbar/2$ (ref. 7). Using this theoretical description, the precise knowledge of the momentum width of a particle σ_p implies a corresponding uncertainty in the extent of its spatial wavefunction σ_x. When the object loses its ability to maintain coherence through interactions with the complex environmental bath, its position is localized. This localization of quantum objects heavily depends on the specific environment they are subjected to[8]. Recent efforts have primarily focused on constructing increasingly large coherent quantum systems[9,10] and other highly delocalized objects to push measurement and other applications to—and beyond—the standard quantum limit[11,12]. Such experiments are at the frontiers of quantum science and engineering and aim, in part, to probe the interface between classical and quantum mechanics.

Here, by contrast, we present a new measurement concept: using highly localized unstable systems embedded in a complex solid-state material at a low temperature as a precision laboratory to probe the quantum properties of subatomic particles. We show that this concept is particularly powerful for investigating the properties of systems that are otherwise not directly accessible because of weak couplings in the Standard Model of particle physics, particularly the neutrino (ν).

Neutrinos are light, neutral leptons, and the only particles in the Standard Model that have an intrinsic chirality, in that they only interact through left-handed currents of the weak interaction through three flavour eigenstates, namely, ν_e, ν_μ and ν_τ. Neutrino oscillation experiments over the last 30 years[13,14] have also indicated that these flavour eigenstates include at least two non-zero mass eigenstates. This observation of non-zero neutrino masses was awarded the Nobel Prize in Physics (2015), but it is still not known how the Standard Model

[1]Department of Physics, Colorado School of Mines, Golden, CO, USA. [2]Facility for Rare Isotope Beams, Michigan State University, East Lansing, MI, USA. [3]TRIUMF, Vancouver, British Columbia, Canada. [4]LIBPhys-UNL, Departamento de Física, Faculdade de Ciências e Tecnologia, NOVA FCT, Universidade Nova de Lisboa, Caparica, Portugal. [5]Université de Strasbourg, CNRS, Institut de Physique et Chimie des Matériaux de Strasbourg, UMR 7504, Strasbourg, France. [6]Lawrence Livermore National Laboratory, Livermore, CA, USA. [7]STAR Cryoelectonics LLC, Santa Fe, NM, USA. [8]Shared Instrumentation Facility, Colorado School of Mines, Golden, CO, USA. [9]XIA LLC, Oakland, CA, USA. [10]LPC Caen, ENSICAEN, Université de Caen, Caen, France. [11]Department of Physics and Astronomy, McMaster University, Hamilton, Ontario, Canada. [12]Université Paris-Saclay, CEA, List, Laboratoire National Henri Becquerel (LNE-LNHB), Palaiseau, France. [13]Pacific Northwest National Laboratory, Richland, WA, USA. ✉e-mail: joseph.smolsky@mines.edu; kleach@mines.edu

should be extended to incorporate massive neutrinos[15]. The flavour oscillation effect for neutrinos arises from the fact that the mass eigenstates and weak-interaction eigenstates are not equal to each other, and because of their small interaction probabilities with the weak and gravitational forces, they are able to maintain coherence for long distances[16]. Thus, even for a neutrino created with a definite flavour—the electron neutrino (ν_e) in weak nuclear decay, for example—a coherent superposition of states exists in the neutrino wavepacket that affects the probability for observing a particular flavour as a function of time or distance from the source. As neutrinos propagate in space, their mass eigenstates separate owing to their different velocities, and eventually no longer overlap resulting in the decoherence of the group wavepacket[17–20].

As neutrinos rarely interact with matter, they are notoriously difficult to detect. For example, a ν_e with 1 MeV kinetic energy has an interaction cross-section of roughly 10^{-42} cm^2 (ref. 21). This fact also makes neutrinos attractive systems to study the fundamental properties of quantum mechanics and exotic new physics, because they are able to maintain coherence for long distances. Historically, observing these so-called 'ghost particles' from various sources requires large volume detectors with limited detection precision that run for several years[22]. These detectors rely on neutral-current and charged-current interactions with an atomic nucleus or electron in these large volumes[21]. The final-state particles are used to reconstruct the incoming neutrino energy and interaction point, along with the neutrino flavour for charged-current interactions. A deficit or excess flux of any flavour in the detector, compared with the flavour ratios at the source, is used to determine the oscillation probabilities as a function of energy and distance. Global data from neutrino oscillation experiments have been used to determine the mass splittings and mixing parameters for the three Standard Model neutrinos[15]. Moreover, data from the Daya Bay[23,24], RENO[25,26] and KamLAND[27] reactor neutrino experiments currently provide loose indirect constraints on the spatial extent of $\bar{\nu}_e$ wavepackets from β^- decay sources[5,6]; however, ν_e wavepackets from electron-capture (EC) sources have never been studied.

To extract physics from the reactor oscillation experiments above, interpretation in the lepton mixing framework of the Standard Model is required[15]. Neutrino mixing parameters, matter effects and combining detector systematic uncertainties make extracting limits on $\sigma_{\nu,x}$ a complex and difficult task. The current limits on wavepackets from reactor $\bar{\nu}_e$ using this approach are 2.1×10^{-13} m $\leq \sigma_{\nu,x} \leq 2$ m (refs. 5,6). If the spatial widths of the $\bar{\nu}_e$ and ν_e wavepackets are indeed near the low end of these limits, it has a considerable impact on the neutrino physics landscape, including alleviating tension in models for sterile neutrinos with electronvolt-scale masses through model-dependent fits to the available data[28,29] and impacting the physics goals of JUNO[30].

Given the current pervading anomalies in the neutrino physics landscape[31], there is a need for new techniques that can provide model-independent access to the neutrino. Clever new experimental concepts have been presented to address this need using efficient, small-scale setups[32–34] that are less model dependent and not limited by low neutrino interaction cross-sections. These experiments aim to precisely measure the low-energy recoiling atoms in nuclear EC decay[35] to access information of the neutrino directly through its entanglement in the final state of radioactive decay. Of these new concepts, the beryllium EC in superconducting tunnel junctions (BeEST) experiment[32] is currently the only one to practically use the concept of direct EC daughter recoil detection for neutrino physics[36] and astrophysics[37]. Here we report, to our knowledge, the first direct limit on the spatial width of a neutrino wavepacket from the energy width of the recoiling nucleus in EC decay, $\sigma_{N,E}$, through their mutual entanglement.

Nuclear EC decay is a radioactive decay mode that results from the capture of an orbital electron by a proton in the nuclear volume[35]. At the fundamental level, this weak-interaction process transmutes an up quark to a down quark through the exchange of a W boson in a constituent nucleon and conserves the lepton number through the emission of ν_e. In the experimental context of the work presented here, the observable final state only contains two products: the recoiling heavy daughter system and ν_e. This simple two-body system that we observe is entangled at its creation, and thus, a precision measurement of the daughter recoil provides direct access to information on the neutrino.

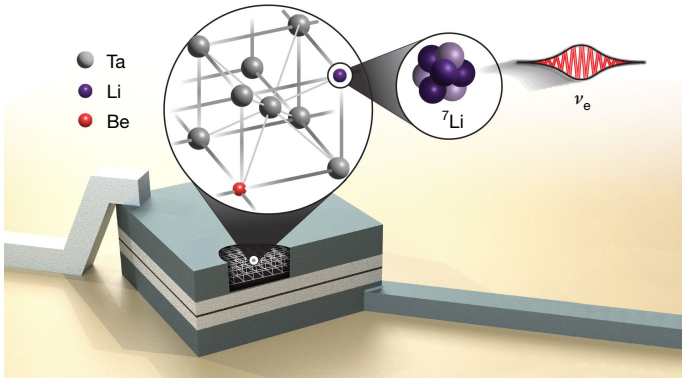

Fig. 1 | ^{7}Be EC in an STJ. Schematic of the STJ sensor showing the five layers described in the text. The ^{7}Be radioactive source is sparsely implanted into the Ta lattice of the absorber layer. The zoomed-in image (top right) shows the final state after EC decay including ^{7}Li recoil and ν_e.

The magnitude of $\sigma_{\nu,x}$ is expected to depend on environmental factors, the type of decay and the scale of localizing interactions. Predictions based on localization through atomic interactions lead to an estimate of $\sigma_{\nu,x} \approx 200$ nm for $\bar{\nu}_e$ from reactor β^- decay sources and $\sigma_{\nu,x} \approx 1$–10 μm for ν_e from a ^{51}Cr EC source[1,3]. Other theoretical approaches that assume localization through degrees of freedom in the nucleus for β^- decay $\bar{\nu}_e$ and degrees of freedom in the atom for EC ν_e lead to $\sigma_{\nu,x} \approx 10$–400 pm for reactor β^- decay sources and $\sigma_{\nu,x} \approx 3$ nm for a beryllium-7 (^{7}Be) EC source[2,4]. As these predictions vary by several orders of magnitude, a precise-enough wavepacket measurement from any nuclear-decay-based ν source could potentially distinguish between these competing theories on the scale of quantum localization in weak nuclear decays.

With seven nucleons and four electrons, the neutron-deficient ^{7}Be nucleus is the simplest pure EC decaying system in the nuclear landscape. To measure the ^{7}Be EC decay spectrum to high precision, we directly embedded the ^{7}Be into the top tantalum film of a single superconducting tunnel junction (STJ) that was used as a high-energy-resolution sensor[38]. The STJ pixel used in this analysis was part of a 36-pixel array in which each sensor had a surface area of 208×208 μm^2 and consisted of the following five layers (from top to bottom): Ta (165 nm)—Al (50 nm)—Al_2O_3 (1 nm)—Al (50 nm)—Ta (265 nm) (Fig. 1). This device was fabricated by photolithography at STAR Cryoelectronics[39]. STJs exploit the small energy gap in superconducting Ta ($\Delta_{Ta} \approx 0.7$ meV) to provide an intrinsic device energy resolution of 1–2 eV in the energy region of interest (approximately 100 eV).

Radioactive ^{7}Be$^+$ ions were directly implanted into the STJ pixel through apertures in a Si collimator that was situated approximately 100 μm above the chip. The ^{7}Be$^+$-ion beam was produced and delivered to the implantation chamber endstation at the TRIUMF-ISAC facility[40] at an energy of 30 keV. The isotopically pure (almost 90%) ^{7}Be$^+$ beam was produced using the isotope separation on-line technique[41] using spallation reactions from a 10 μA, 480 MeV proton beam incident on a stack of thin uranium carbide targets. Once released from the target through diffusion, the created beryllium atoms were selectively ionized using the ion guide laser ion source[42] operated in suppression mode[43]. The resulting beam of ^{7}Be$^+$ ions was implanted at a rate of 6.1×10^6 s^{-1} for a period of 25 h to generate an initial per-pixel activity

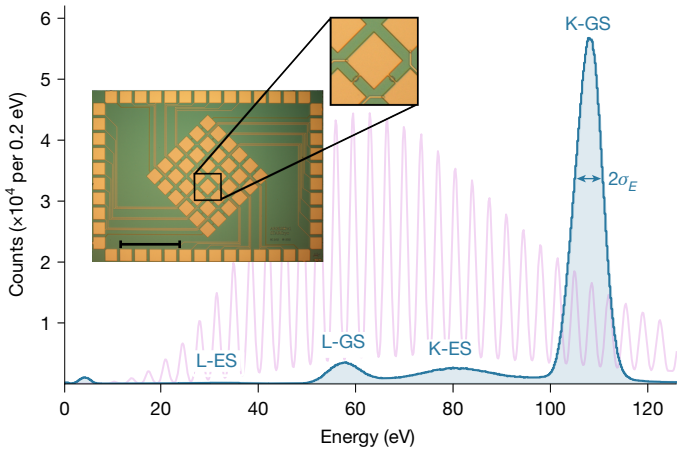

Fig. 2 | The STJ array of the BeEST experiment and precision energy measurement. The measured ^{7}Li recoil spectrum with the four peaks described in the text for 20 h of data from the single STJ pixel shown in the inset. The L-ES peak is barely visible because of its weak population probability. The measured uncertainty of the K-GS peak is shown, and is conservatively extracted as the upper limit on the inherent energy width of the recoil, $\sigma_{N,E} \leq 2.9$ eV, through the procedure described in the text. The comb of the peaks from the calibration laser spectrum (violet) is also shown for comparison. The small bump in the spectrum at 4 eV results from a non-prompt, decay-induced process, the source of which is still under investigation. Scale bar, 1 mm.

in the STJs of roughly 50 Bq. After implantation, the chip was cleaned and processed at TRIUMF to remove loose and surface-deposited activity and subsequently shipped to Lawrence Livermore National Laboratory (LLNL).

The final-state energy spectrum from the decay of ^{7}Be was measured at LLNL with the STJ detector at a temperature of approximately 0.1 K in a two-stage adiabatic demagnetization refrigerator with liquid-nitrogen and liquid-helium precooling. Signal traces were read out continuously at a rate of 1.25 MSa s^{-1} at a 16-bit resolution using a PXIe-6356 analogue-to-digital converter. For the real-time in situ monitoring of the response and energy calibration, the STJs were simultaneously exposed to 3.49865(15) eV photons from a pulsed, 355 nm frequency-tripled Nd:YVO_4 laser triggered at a rate of 100 Hz that was fed into the cold stage of the adiabatic demagnetization refrigerator through a fibre to illuminate the pixels. The laser intensity was adjusted such that multi-photon absorption provided a comb of peaks in the energy range from 20 eV to 120 eV. The energy resolution of the laser peaks was 1.85(1) eV at 108.5 eV with residuals of approximately 0.02 eV in the region of interest[44,45]. Selected data (Fig. 2) were acquired for approximately 20 h on 6 November 2022, which are a small subset of the full BeEST Phase-III dataset.

^{7}Be decays to lithium-7 (^{7}Li) and a ν_e with a half-life of $T_{1/2} = 53.22(6)$ days[46] and a total decay energy of $Q_{EC} = 861.963(23)$ keV (ref. 47). In the EC process, the electron can be captured either from the 1*s* shell (*K* capture) or the 2*s* shell (*L* capture) of Be, with a measured *L*/*K* ratio of 0.070(7) (ref. 37). For *K* capture, the binding energy of the 1*s* hole is subsequently liberated by the emission of an Auger electron[48]. A small branch of 10.44(4)% results in the population of a short-lived excited nuclear state in ^{7}Li ($T_{1/2} = 72.8(20)$ fs) that de-excites by the emission of a 477.603(2) keV γ-ray[46]. As the nuclear decay and subsequent atomic relaxation occur on short timescales, our measurement method results in a low-energy spectrum with four peaks: two for *K* capture and two for *L* capture into the ground state (GS) and excited state (ES) of ^{7}Li, all of which are well resolved. The two recoil peaks from the ES decay of ^{7}Li are Doppler broadened from γ decay in flight[37,38].

The final ^{7}Be decay spectrum (Fig. 2) includes events from a single pixel that were not in coincidence with the laser logic pulse or simultaneous signals in other pixels. The latter of these two criteria was imposed to remove the large, low-energy background from 478 keV γ-ray Compton scattering interactions in the 0.5 mm Si substrate below the STJ array, which generated signals in many pixels simultaneously. The resulting EC recoil spectrum is dominated by the four expected peaks arising from the two atomic and two nuclear processes described above. A sophisticated analysis of the spectrum, which includes higher-order processes such as atomic shake-up and shake-off effects, is ongoing for the beyond-Standard Model physics search program of the BeEST experiment, but is not required here.

Only the K-GS peak is used in this analysis because it provides the highest statistical significance for a measurement of the recoil energy width with the smallest uncertainty and does not have Doppler broadening as the ES peaks do. The width of the K-GS recoil peak (Fig. 2) is broadened beyond the intrinsic resolution of the sensors based on the resolution of the laser peaks. Some of this width is because of structural and chemical variations of the Li 1*s* binding energy at different sites in the Ta lattice, which contribute $\mathcal{O}$(1 eV) to the broadening[49]. However, owing to their complexity and the fact that these effects are not yet quantified in detail for the BeEST energy spectrum, we conservatively attributed all of the measured broadening in the K-GS peak to quantum uncertainty. This also ignores the negligible broadening caused by decays at the edges of the pixel[50]. A future analysis that accounts for known causes of broadening will improve the limits presented here.

The K-GS peak was fit in the region from 101 eV to 115 eV (Fig. 2) with a single Voigt function to extract the energy uncertainty width $\sigma_{N,E} \leq 2.9$ eV at the 95% confidence level (CL) using the profile likelihood method[51–53]. We then converted the full energy width to a momentum width of the ^{7}Li recoil. The uncertainty was propagated using $\sigma_p = \sqrt{m/2E}\,\sigma_E$, where m is the atomic mass of ^{7}Li and E is energy of the K-GS peak centroid, resulting in $\sigma_{Li,p} \leq 16$ keV c^{-1}. Contributions due to the uncertainty in measurements of m are negligible[54]. Finally, using the Heisenberg uncertainty relation, we extracted a lower limit on the spatial width on the nuclear recoil of $\sigma_{N,x} \geq 6.2$ pm. These results are based on our measurement of the K-GS peak energy width under the experimental conditions reported here and have no underlying assumptions about the scale of localization. Differences in the expected broadening owing to more realistic non-Gaussian wavepackets are negligible compared with other causes of variations in the broadening mentioned previously[2].

To extract a limit on the neutrino spatial width $\sigma_{\nu,x}$, two approaches were used: one based on the conservation of energy[1] and the other based on the conservation of momentum[2]. In the first method, the neutrino energy width is equivalent to that of the entangled recoil nucleus, which, in our case, is the upper limit on the measured energy width $\sigma_{\nu,E} = \sigma_{N,E} \leq 2.9$ eV. This limit was then converted into a momentum uncertainty using the relativistic energy–momentum relation $p_\nu = E_\nu/c$ and $\sigma_p = \sigma_E/c$. The spatial uncertainty was extracted as $\sigma_{\nu,x} \geq 34$ nm at the 95% CL using the uncertainty principle. As our conservative method includes effects from sources of inhomogeneous broadening mentioned previously, the actual homogeneous broadening related to quantum uncertainty is expected to be markedly smaller than this limit. We also note that this method is equivalent to the approach prescribed in ref. 17 in which the uncertainty in energy comes from the inverse of the time for which wavepackets overlap at production, which depends on the velocities of the nuclei in the source. Our measured upper limit on the energy uncertainty is approximately 3–10 times larger than predictions from models based on atomic-scale localization and uncertainty in the time between atomic interactions in the reactor and ^{51}Cr sources[1,3]. Extending these theoretical models to make predictions for neutrinos emitted from nuclear decays in a sub-kelvin crystal lattice, as in the BeEST experiment, is beyond the scope of the present work.

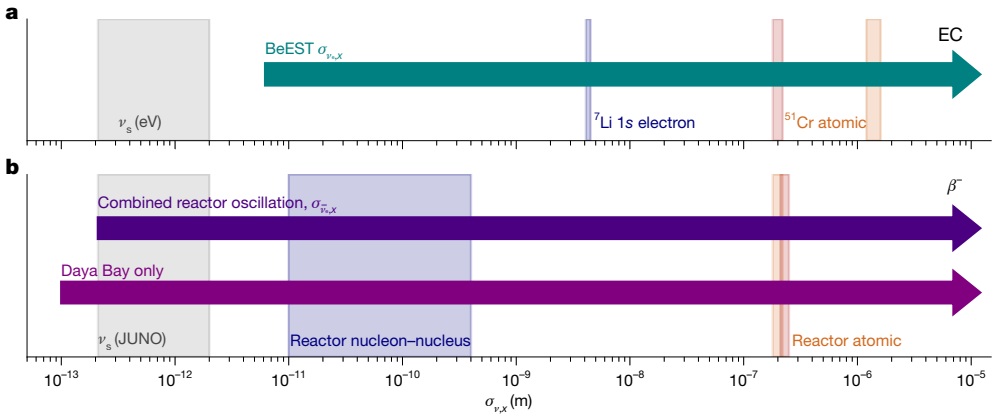

Fig. 3 | Experimental limits and theoretical predictions for radioactive-decay-based neutrino sources. a,**b**, Comparison between experimental limits (horizontal bars) and theoretical estimates (vertical bars) for the spatial extent of a neutrino wavepacket created in EC sources (**a**) and reactor β^- sources (**b**). This plot encapsulates the current status of the spatial uncertainties of the neutrino wavepacket in both experiment and theory from the literature. For EC sources in **a**, the theoretical predictions are based on different scales of localization for ν_e. The blue band is based on the conservation of momentum and subatomic localization determined by the momentum uncertainty of the ^{7}Li 1*s* electron orbital[4]. The red and orange bands are from two different predictions for atomic localization in a hot ^{51}Cr source[1,3]. For the reactor sources in **b**, the experimental limits are indirectly inferred from various oscillation experiments[5,6]. The blue band from 10 pm to 400 pm is the theoretical estimate based on nucleon-scale/nucleus-scale localization estimates[2]. The orange and red bands are estimates based on localization by atomic interactions in the reactor local environment[1,3]. The bands on the far left spanning both plots correspond to the scenario in which the widths of the neutrino wavepackets are preferred in electronvolt-scale ν_s model fits to data[28,29], and in the case of reactor sources, would also be the region that wavepacket separation would be visible in JUNO[6,30].

For the second approach[2], the momentum widths of the recoiling nucleus and neutrino are equivalent, that is, $\sigma_{\nu,p} = \sigma_{\mathrm{Li},p} \leq 16$ keV c^{-1}, and the uncertainty principle again gives the spatial width. Under this approach, we determine a lower limit on the spatial width of the neutrino of $\sigma_{\nu,x} = \sigma_{\mathrm{N},x} \geq 6.2$ pm at the 95% CL (Fig. 3a). As the two methods described above yield markedly different results for the widths of the neutrino wavepackets (details of which are discussed extensively in the literature[1–4,17]), we do not claim the validity of one over the other here. We instead use the more conservative of the two to set our reported lower limits. The result is equivalent to combining the momentum and energy uncertainties as proposed in refs. 3,19,20.

Establishing an experimental distinction between localization models, particularly for a purely weak-interaction-mediated transition under the emission of a neutrino, would be a quantitative test of scale decoupling in quantum field theory[55], and may perhaps be the most important application of this technique in the future. For example, if the localizing interactions in weak nuclear decay are at the subatomic scale because of internal degrees of freedom in the nucleus[2,4], the resulting wavepackets are expected to be several orders of magnitude smaller than if the decay product widths are set by atomic interactions[1,3] (Fig. 3). A measurement precise enough to distinguish between these scenarios is expected to apply to all nuclear-decay-based ν sources and could serve as a fundamental test of quantum mechanics.

To perform a measurement that can distinguish the above models, our presented technique requires improvements and refinement in both analysis and detection methods. Potential improvements could come from accounting for known sources of broadening and minimizing lattice effects with more uniform superconducting films. We have shown that this technique can be applied to nuclear recoils of EC decay sources, but it may be possible to adapt it for the precision measurements of nuclear recoils of $\beta^{\pm}$ decay sources in STJs with the upcoming Superconducting Array for Low-Energy Radiation experiment at the Facility for Rare Isotope Beams. As nuclear β decay does not involve the capture of an orbital electron in the initial state, it could enable a direct comparison with β^- sources and shed light on some of the fundamental questions on localization posed above (Fig. 3b).

The lower limit on the neutrino spatial width presented here does, however, provide potential insight into the suggestion that wavepacket separation may relieve tension in electronvolt-scale ν_s model fits with reactor experiments and the so-called 'gallium anomaly' in EC decay oscillation experiments. This improvement does, nevertheless, rely on the assumption that $\sigma_{\nu,x}$ varies negligibly between reactor β decay $\bar{\nu}_e$ sources and ^{51}Cr ν_e EC sources[28]. The same approach was also used to show that wavepacket separation could be one of the potential causes of the dampening-like effect that improves electronvolt-scale ν_s fits to global data[29]. The impact of wavepacket separation in these fits is marked near the current experimental lower limit from the reactor data of $\sigma_{\nu,x} \geq 210$ fm but becomes indistinguishable from the plane-wave approximation at $\sigma_{\nu,x} \geq 2$ pm (ref. 28). Our limit of $\sigma_{\nu,x} \geq 6.2$ pm for an EC source, as shown in Fig. 3a along with the region favoured by ν_s models, disfavours wavepacket separation as the correct explanation for this anomaly, unless the reactor and ^{51}Cr sources both produce ν much more localized than the BeEST ^{7}Be source. The region preferred by ν_s models also corresponds to the sensitivity region of JUNO[6,30]. However, JUNO will detect $\bar{\nu}_e$ from nuclear reactors, and how this relates to an EC measurement depends on environmental factors and the scale of localization[1–4].

In summary, we present a new experimental concept to measure the low-energy recoiling daughter system from highly localized EC decaying rare isotopes inside superconducting sensors. Using this method, we have been able to directly constrain the quantum localization scale of the final-state system in electroweak nuclear decay. Here we report a conservative upper limit of the energy width of the recoiling ^{7}Li system from the EC decay of ^{7}Be in a tantalum matrix at 0.1 K of $\sigma_{\mathrm{N},E} \leq 2.9$ eV (95% CL). This corresponds to a limit on the spatial width of the ^{7}Li nuclear recoil of $\sigma_{\mathrm{N},x} \geq 6.2$ pm, which suggests that the localization of the final-state system occurs at a scale much larger than the nucleus in which the interaction occurs. From this measurement, we also set the same limit on the spatial width of the entangled neutrino, $\sigma_{\nu,x} \geq 6.2$ pm, to our knowledge the first such limit on any EC ν_e source thus far and the first limit set by the direct measurements of the ν source. This limit disfavours wavepacket separation as the cause of dampening preferred by electronvolt-scale ν_s model fits to anomalous data. With planned future improvements to the analysis and detectors, this technique may be able to distinguish between competing models of localization in weak nuclear decays, and may provide a fundamental test of quantum mechanics.

Online content

Any methods, additional references, Nature Portfolio reporting summaries, source data, extended data, supplementary information, acknowledgements, peer review information; details of author contributions and competing interests; and statements of data and code availability are available at https://doi.org/10.1038/s41586-024-08479-6.

1. Akhmedov, E. & Smirnov, A. Y. Damping of neutrino oscillations, decoherence and the lengths of neutrino wave packets. *J. High Energy Phys.* **2022**, 82 (2022).
2. Jones, B. J. P., Marzec, E. & Spitz, J. Width of a beta-decay-induced antineutrino wave packet. *Phys. Rev. D* **107**, 013008 (2023).
3. Krueger, R. & Schwetz, T. Decoherence effects in reactor and Gallium neutrino oscillation experiments: a QFT approach. *Eur. Phys. J. C* **83**, 578 (2023).
4. Jones, B. J. P., Marzec, E. & Spitz, J. The width of an electron-capture neutrino wave packet. Preprint at http://arxiv.org/abs/2404.19746v1 (2024).
5. Daya Bay Collaboration Study of the wave packet treatment of neutrino oscillation at Daya Bay. *Eur. Phys. J. C* **77**, 606 (2017).
6. Gouvêa, A., De Romeri, V. & Ternes, C. A. Combined analysis of neutrino decoherence at reactor experiments. *J. High Energy Phys.* **2021**, 42 (2021).
7. Heisenberg, W. Über quantentheoretische Umdeutung kinematischer und mechanischer Beziehungen. *Z. Phys.* **33**, 879–893 (1925).
8. Abanin, D. A., Altman, E., Bloch, I. & Serbyn, M. Colloquium: many-body localization, thermalization, and entanglement. *Rev. Mod. Phys.* **91**, 021001 (2019).
9. Fein, Y. Y. et al. Quantum superposition of molecules beyond 25 kDa. *Nat. Phys.* **15**, 1242–1245 (2019).
10. Bild, M. et al. Schrödinger cat states of a 16-microgram mechanical oscillator. *Science* **380**, 274–278 (2023).
11. Beckey, J., Carney, D. & Marocco, G. Quantum measurements in fundamental physics: a user's manual. Preprint at http://arxiv.org/abs/2311.07270 (2023).
12. Bass, S. D. & Doser, M. Quantum sensing for particle physics. *Nat. Rev. Phys.* **6**, 329–339 (2024)
13. Fukuda, Y. et al. Evidence for oscillation of atmospheric neutrinos. *Phys. Rev. Lett.* **81**, 1562–1567 (1998).
14. Ahmad, Q. R. et al. Measurement of the rate of $\nu_e + d \rightarrow p + p + e^-$ interactions produced by ^{8}B solar neutrinos at the Sudbury Neutrino Observatory. *Phys. Rev. Lett.* **87**, 071301 (2001).
15. Navas, S. et al. Review of particle physics. *Phys. Rev. D* **110**, 030001 (2024).
16. Abbasi, R. et al. Search for decoherence from quantum gravity with atmospheric neutrinos. *Nat. Phys.* **20**, 913–920 (2024)
17. Beuthe, M. Oscillations of neutrinos and mesons in quantum field theory. *Phys. Rep.* **375**, 105–218 (2003).
18. Kayser, B. On the quantum mechanics of neutrino oscillation. *Phys. Rev. D* **24**, 110–116 (1981).
19. Akhmedov, E. Quantum mechanics aspects and subtleties of neutrino oscillations. Preprint at https://arxiv.org/abs/1901.05232 (2019).
20. Giunti, C. & Kim, C. W. Coherence of neutrino oscillations in the wave packet approach. *Phys. Rev. D* **58**, 017301 (1998).
21. Formaggio, J. A. & Zeller, G. P. From eV to EeV: neutrino cross sections across energy scales. *Rev. Mod. Phys.* **84**, 1307–1341 (2012).
22. Di Lodovico, F., Patterson, R. B., Shiozawa, M. & Worcester, E. Experimental considerations in long-baseline neutrino oscillation measurements. *Annu. Rev. Nucl. Part. Sci.* **73**, 69–93 (2023).
23. Cao, J. & Luk, K.-B. An overview of the Daya Bay reactor neutrino experiment. *Nucl. Phys. B* **908**, 62–73 (2016).
24. An, F. P. et al. First measurement of high-energy reactor antineutrinos at Daya Bay. *Phys. Rev. Lett.* **129**, 041801 (2022).
25. RENO Collaboration. RENO: an experiment for neutrino oscillation parameter θ_{13} using reactor neutrinos at Yonggwang. Preprint at https://arxiv.org/abs/1003.1391 (2010).
26. Ahn, J. K. et al. Observation of reactor electron antineutrinos disappearance in the RENO experiment. *Phys. Rev. Lett.* **108**, 191802 (2012).
27. The KamLAND Collaboration Constraints on θ_{13} from a three-flavor oscillation analysis of reactor antineutrinos at KamLAND. *Phys. Rev. D* **83**, 052002 (2011).
28. Argüelles, C. A., Bertólez-Martínez, T. & Salvado, J. Impact of wave packet separation in low-energy sterile neutrino searches. *Phys. Rev. D* **107**, 036004 (2023).
29. Hardin, J. M. et al. New clues about light sterile neutrinos: preference for models with damping effects in global fits. *J. High Energy Phys.* **2023**, 58 (2023).
30. JUNO collaboration Damping signatures at JUNO, a medium-baseline reactor neutrino oscillation experiment. *J. High Energy Phys.* **2022**, 62 (2022).
31. Schoppmann, S. Status of anomalies and sterile neutrino searches at nuclear reactors. *Universe* **7**, 360 (2021)
32. Leach, K. G., Friedrich, S. & BeEST Collaboration The BeEST experiment: searching for beyond Standard Model neutrinos using ^{7}Be decay in STJs. *J. Low Temp. Phys.* **209**, 796–803 (2022).
33. Martoff, C. J. et al. HUNTER: precision massive-neutrino search based on a laser cooled atomic source. *Quantum Sci. Technol.* **6**, 024008 (2021).
34. Carney, D., Leach, K. G. & Moore, D. C. Searches for massive neutrinos with mechanical quantum sensors. *PRX Quantum* **4**, 010315 (2023).
35. Bambynek, W. et al. Orbital electron capture by the nucleus. *Rev. Mod. Phys.* **49**, 77–221 (1977).
36. Friedrich, S. et al. Limits on the existence of sub-MeV sterile neutrinos from the decay of ^{7}Be in superconducting quantum sensors. *Phys. Rev. Lett.* **126**, 021803 (2021).
37. Fretwell, S. et al. Direct measurement of the ^{7}Be *L*/*K* capture ratio in Ta-based superconducting tunnel junctions. *Phys. Rev. Lett.* **125**, 032701 (2020).
38. Friedrich, S. Superconducting tunnel junction photon detectors: theory and applications. *J. Low Temp. Phys.* **151**, 277–286 (2008).
39. Carpenter, M. H. et al. Development of Ta-based superconducting tunnel junction X-ray detector arrays. *IEEE Trans. Appl. Supercond.* **23**, 2400504–2400504 (2013).
40. Dilling, J. & Krücken, R. The experimental facilities at ISAC. *Hyperfine Interact.* **225**, 111–114 (2014).
41. Blumenfeld, Y., Nilsson, T. & Duppen, P. V. Facilities and methods for radioactive ion beam production. *Phys. Scr.* **2013**, 014023 (2013).
42. Raeder, S. et al. An ion guide laser ion source for isobar-suppressed rare isotope beams. *Rev. Sci. Instrum.* **85**, 033309 (2014).
43. Mostamand, M. et al. Production of clean rare isotope beams at TRIUMF ion guide laser ion source. *Hyperfine Interact.* **241**, 36 (2020).
44. Friedrich, S., Ponce, F., Hall, J. A. & Cantor, R. Non-linearities in superconducting tunnel junction radiation detectors and their MCA readout. *J. Low Temp. Phys.* **200**, 200–205 (2020).
45. Bray, C. et al. The data acquisition system for phase-III of the BeEST experiment. *J. Low Temp. Phys.* https://doi.org/10.1007/s10909-024-03242-7 (2024).
46. Bé, M.-M. et al. *Table of Radionuclides.* Monographie BIPM-5 (Bureau International des Poids et Mesures, 2004).
47. Bhandari, R. et al. First direct ^{7}Be electron-capture *Q*-value measurement toward high-precision searches for neutrino physics beyond the Standard Model. *Phys. Rev. C* **109**, 022501 (2024).
48. Hubbell, J. H. et al. A review, bibliography, and tabulation of *k*, *l*, and higher atomic shell X-ray fluorescence yields. *J. Phys. Chem. Ref. Data* **23**, 339–364 (1994).
49. Samanta, A., Friedrich, S., Leach, K. G. & Lordi, V. Material effects on electron-capture decay in cryogenic sensors. *Phys. Rev. Appl.* **19**, 014032 (2023).
50. Friedrich, S. et al. Characterization of non-uniformities in superconducting tunnel junction radiation detectors. *J. Low Temp. Phys.* **209**, 1063–1069 (2022).
51. Virtanen, P. et al. SciPy 1.0: fundamental algorithms for scientific computing in Python. *Nat. Methods* **17**, 261–272 (2020).
52. Vugrin, K. W., Swiler, L. P., Roberts, R. M., Stucky-Mack, N. J. & Sullivan, S. P. Confidence region estimation techniques for nonlinear regression in groundwater flow: three case studies. *Water Resour. Res.* **43**, W03423 (2007).
53. Royston, P. Profile likelihood for estimation and confidence intervals. *Stata J.* **7**, 376–387 (2007).
54. Wang, M., Huang, W. J., Kondev, F. G., Audi, G. & Naimi, S. The AME 2020 atomic mass evaluation (II). Tables, graphs and references. *Chinese Phys. C* **45**, 030003 (2021).
55. Balasubramanian, V., McDermott, M. B. & Van Raamsdonk, M. Momentum-space entanglement and renormalization in quantum field theory. *Phys. Rev. D* **86**, 045014 (2012).

Data availability

The data are available at Zenodo (https://zenodo.org/records/14182726)[56].

Code availability

The code for extracting the limits is available at Zenodo (https://zenodo.org/records/14182726)[56].

56. Smolsky, J. BeEST single pixel data for conservative wavepacket analysis. *Zenodo* https://doi.org/10.5281/zenodo.14182726 (2024).

Acknowledgements We thank D. Moore, D. Carney, B. Jones, C. Argüelles-Delgado, J. Formaggio and F. Sarazin for useful discussions. The BeEST experiment is funded by the Gordon and Betty Moore Foundation (no. 10.37807/GBMF11571); the US Department of Energy, Office of Science, Office of Nuclear Physics, under award nos. DE-SC0021245 and SCW1758; the LLNL Laboratory Directed Research and Development program through grant nos. 19-FS-027 and 20-LW-006; the European Metrology Programme for Innovation and Research (EMPIR) project nos. 17FUN02 MetroMMC and 20FUN09 PrimA-LTD; and the FCT—Fundação para a Ciência e Tecnologia (Portugal)—through national funds in the framework of the project no. UID/04559/2020 (LIBPhys). TRIUMF receives federal funding through a contribution agreement with the National Research Council of Canada. This work was performed under the auspices of the US Department of Energy by LLNL under contract no. DE-AC52-07NA27344. F.P. is funded as part of the Open Call Initiative at Pacific Northwest National Laboratory and conducted under the Laboratory Directed Research and Development Program. Pacific Northwest National Laboratory is a multiprogram national laboratory operated by Battelle for the US Department of Energy. K.G.L. acknowledges support from the Facility for Rare Isotope Beams (FRIB) while on sabbatical. FRIB is a US Department of Energy, Office of Science User Facility, under award no. DE-SC0000661.

Author contributions J.S. and K.G.L. performed the spectral analysis, derived the wavepacket limits and led the scientific context and discussion for the article. I.K., C.B., A.M., C.S.-W., A. Lamm, K.B., A.G., C.H., J. Taylor and J. Templet performed the data-cleaning procedures and evaluated the systematic effects in the data. P.A., A.A., D.D., M.G., C.N.H, P.-A.H., V.L., J.M., X.M., A.S. and J.P.S. evaluated the atomic and materials effects of the decay as systematic input to the analysis for the BeEST experiment. I.K., C.B., A.M., F.P., G.-B.K., L.M.H. and S. Friedrich compiled the cleaned data, incorporated the known physical effects and prepared it for the final data analysis. S. Friedrich, C.B. and S. Fretwell performed the experiment and collected the data. A. Lennarz, R.A., D.M., C.R., S.U. and L.W. performed the radioactive Be implantation and post-processing of the irradiated STJs. R.C. and A.H. fabricated the STJs. W.K.W. and J.T.H. built the STJ preamplifier. D.M. provided the scientific context for physics beyond the Standard Model in the theory community. K.G.L. and S. Friedrich provided the scientific and technical leadership for the collaboration. All authors have reviewed the paper and the results.

Competing interests The authors declare no competing interests.

Additional information
Correspondence and requests for materials should be addressed to Joseph Smolsky or Kyle G. Leach.
Peer review information *Nature* thanks Valentina De Romeri and the other, anonymous, reviewer(s) for their contribution to the peer review of this work.